Supporting Information

Lattice interconversion of 1D ferrocene-based perovskite induced by solvent molecules for selectively photocatalytic toluene oxidation

Yan-Li Yang,[a#] Ke-Ke Guo,[a,b#] Xue Bai,[a] An-Ge Zhang,[a] Ying Lu, [a] Mao-Chun Zhu,[a] and Shu-Xia Liu [a]*

[a]Key Laboratory of Polyoxometalate and Reticular Material Chemistry of Ministry of Education, Faculty of Chemistry, Northeast Normal University, Changchun, Jilin 130024, P. R. China

[b]Key Laboratory of Eco-Functional Polymer Materials of the Ministry of Education, College of Chemistry and Chemical Engineering, Northwest Normal University, Lanzhou, Gansu 730070, P.R. China

[#]Y. Yang and K. Guo contributed equally to this work.

Email: liusx@nenu.edu.cn

Materials and methods.

All chemical reagents and solvents were available commercially and used without further purification. PbI_2 (98%) and N,N-Dimethylaminomethylferrocene ($C_{13}H_{17}FeN$) (99%) were purchased from Energy Chemical. Hydroiodic acid (HI, 55%-58%), N,N-Diethylformamide (DEF,99%), toluene (99%), *o*-xylene (98%), *m*-xylene (99%), *p*-xylene (99%), *p*-chlorotoluene (98%), 4-fluorotoluene (98%) and p-bromotoluene (99%) were purchased from Aladdin.

Powder X-ray diffraction (PXRD) patterns were were collected on a Smartlab instrument using Cu Kα radiation (λ = 1.5418 Å) in the 2θ range 5-50° at a scan rate of 10° min^{-1}. The solid diffuse reflectance UV-vis spectra of $(C_{13}H_{17}FeNH)PbI_3$ and $(C_{13}H_{17}FeNH)PbI_3$❿DEF were measured on a Cary7000 UV-Vis-NIR Spectrophotometer from 200 to 800 nm at room temperature. A barium sulfate ($BaSO_4$) pellet was used as the standard with 100% reflectance. The steady-state photoluminescence (PL) emission spectroscopy, the temperature-dependent PL as well as the time-resolved photoluminescence (TRPL) spectra were measured by FLS980 with a 375 nm and 405 nm excitation light, respectively. The photoelectrochemical experiments were performed using a CHI 660 electrochemical workstation (Shanghai Chenhua Instrument Corp. China) at room temperature. A three-electrode system was employed in a quartz cell with a Pt wire as the counter electrode, a saturated calomel electrode (SCE) as the reference electrode, and the composite film-assembled FTO glass as the working electrode. The illumination area of working electrodes was set constant at 1.0 × 1.0 cm^2. The transient photocurrent experiment was carried out at a

constant bias of 0.5 V under simulated sunlight irradiation conditions (300 W Xenon arc lamp, $\lambda > 420$ nm, 500 $mW \cdot cm^{-2}$) upon on-off cycling irradiation. Mott-Schottky plots was collected by measuring Impedance-Potential curves at the fixed frequency of 500 Hz and 1000 Hz, respectively. An aqueous solution of 0.5 M Na_2SO_4 was used as the electrolyte throughout the experiments. The obtained potential (vs. SCE) was converted to E_{RHE} (E_{NHE} at pH = 0) by the equation $E_{RHE} = E_{SCE} + 0.0592pH + 0.241$.[1]

X-Ray Crystallography

The crystallographic data of $(C_{13}H_{17}FeNH)PbI_3$ and $(C_{13}H_{17}FeNH)PbI_3$❿DEF were collected at 298.15 K using a Bruker Apex CCD diffractometer with Mo-Kα radiation (λ=0.71073 Å). By using SHELX programs via Olex2 interface,[1-2] the crystal structure of these two perovskite single crystals were solved by direct methods and further refined by full-matrix least-squares methods. All hydrogen atoms were placed in calculated positions and refined by using a riding model. All non-hydrogen atoms were refined anisotropically. The crystallographic data of $(C_{13}H_{17}FeNH)PbI_3$❿DEF and $(C_{13}H_{17}FeNH)PbI_3$ have been deposited in the Cambridge Crystallographic Data Centre with CCDC numbers 2416757 and 2379877, respectively. Pertinent crystal data and relevant refinement parameters for $(C_{13}H_{17}FeNH)PbI_3$ and $(C_{13}H_{17}FeNH)PbI_3$❿DEF are listed in Table S1.

Density functional theory (DFT) calculations

The calculations were carried out using the DMOL3 (Density Functional Theory based Quantum Chemistry) software package. The Perdew-Burke-Ernzerhof (PBE) functional was used within the generalized gradient approximation (GGA). The double numerical plus polarization (DNP) basis set was employed for all atoms in the cluster. The orbital cutoff was set to 3.5 Å to ensure accurate treatment of the electron density near the cluster boundary. The energy convergence criterion was set to 10 e^{-5} eV/atom, the force convergence criterion was set to 0.002 eV/Å, and the maximum displacement criterion for geometry optimization was set to 0.005 Å. All calculations included spin polarization to accurately describe the magnetic properties of the system. For the geometry optimization, the BFGS algorithm was used.

AQE experiments

The apparent quantum efficiency (AQE) was conducted with a 365 nm LED light source (Perfectlight, PLS-LED) for 4 h. The average irradiation intensity was determined by a optical power meter. The number of incident photons (N) and AQE are calculated with the following equation.

$$N = \frac{E\lambda}{hc} = \frac{I \times A \times t \times \lambda}{hc}$$

$$N = \frac{number\ of\ reacted\ photogenerated\ holes}{nuber\ of\ incident\ photons}$$

$$= \frac{number\ of\ reacted\ toluene}{nuber\ of\ incident\ photons} = \frac{nN_A}{N}$$

Where I represents the light intensity of the 356 nm LED sorce, A is the irradiation area of reaction system, t is the time, λis the wavelength of the light, h represents the Plank

constant, c is the speed of light, n is the amount of toluene reacted, and N_A is the Avogadro constant.

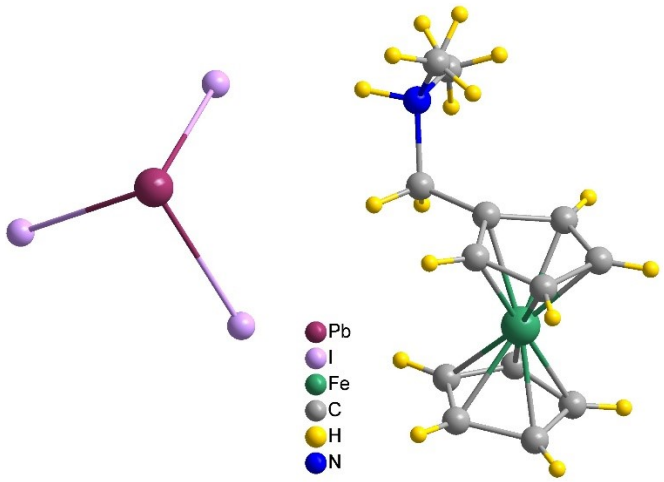

Fig. S1 Basic structural motif of $(C_{13}H_{17}FeNH)PbI_3$.

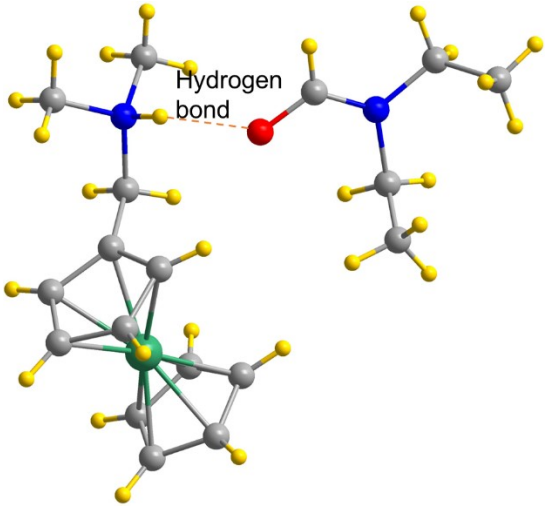

Fig. S2 Hydrogen bonding interaction between DEF and $C_{13}H_{17}FeNH$ in $(C_{13}H_{17}FeNH)PbI_3$❿DEF.

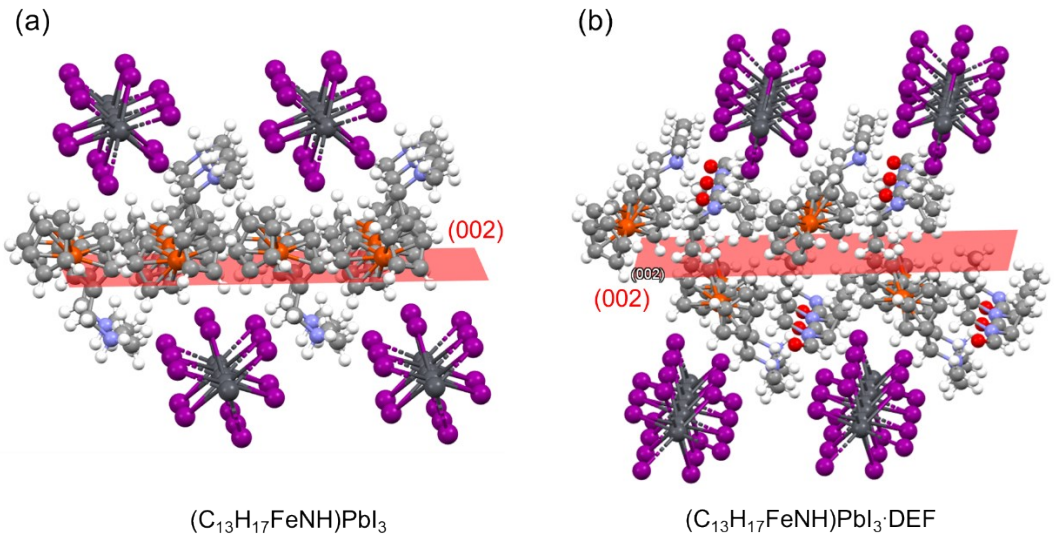

Fig. S3 The (002) crystal plane of $(C_{13}H_{17}FeNH)PbI_3$ (a) and $(C_{13}H_{17}FeNH)PbI_3$❿DEF (b), respectively.

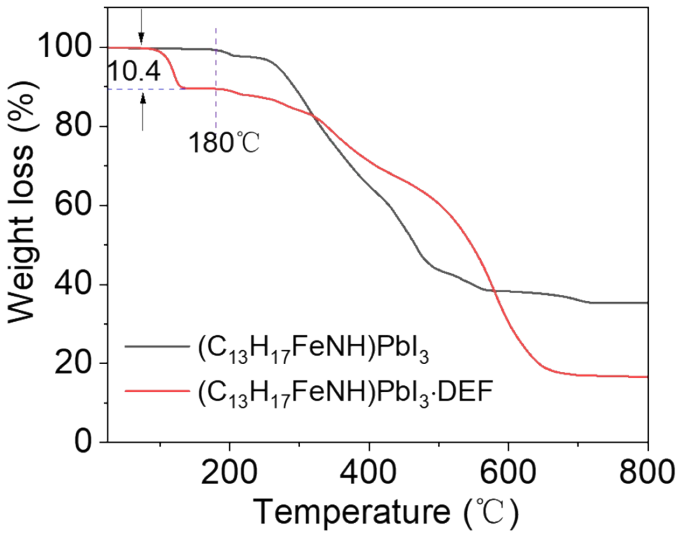

Fig. S4 TGA curves of $(C_{13}H_{17}FeNH)PbI_3$ (a) and $(C_{13}H_{17}FeNH)PbI_3$❿DEF (b), respectively.

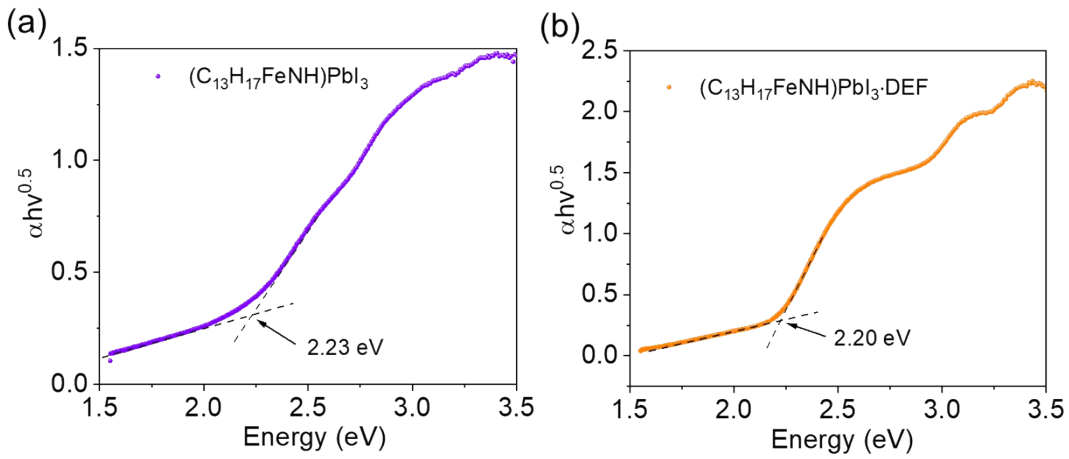

Fig. S5 Tauc plots of $(C_{13}H_{17}FeNH)PbI_3$ (a) and $(C_{13}H_{17}FeNH)PbI_3$❿DEF (b), respectively.

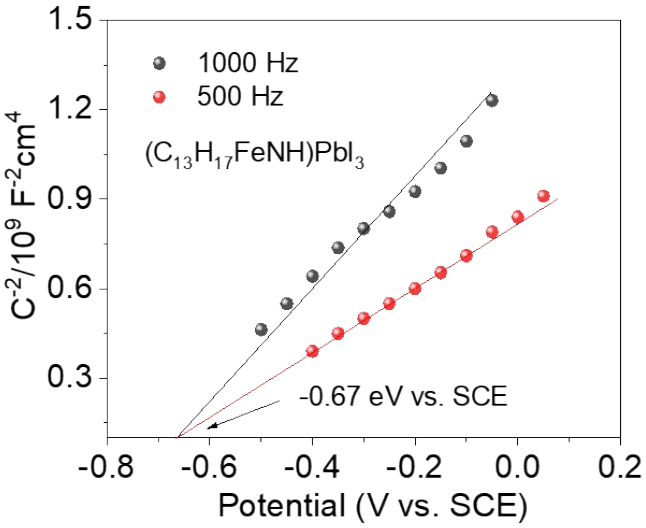

Fig. S6 Mott-Schottky plot of $(C_{13}H_{17}FeNH)PbI_3$ at 500 and 1000 Hz, respectively.

Fig. S7 Mott-Schottky plot of $(C_{13}H_{17}FeNH)PbI_3$❿DEF at 500 and 1000 Hz, respectively.

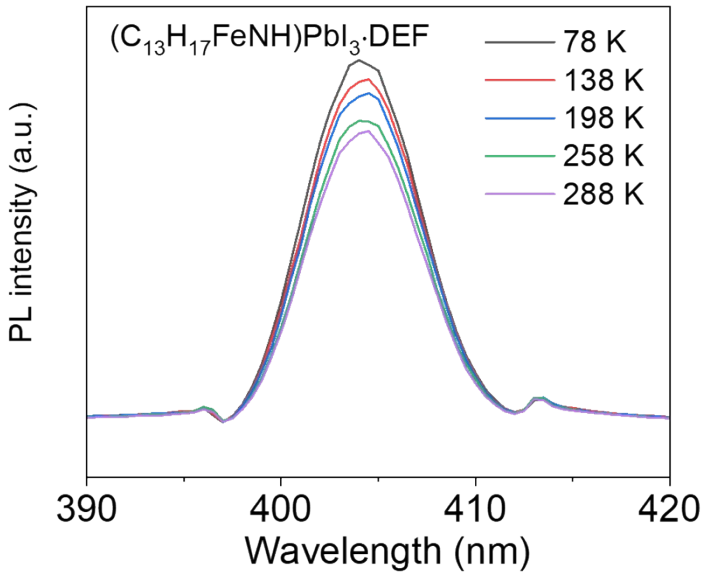

Fig. S8 The temperature-dependent PL intensity plots of $(C_{13}H_{17}FeNH)PbI_3$❿DEF.

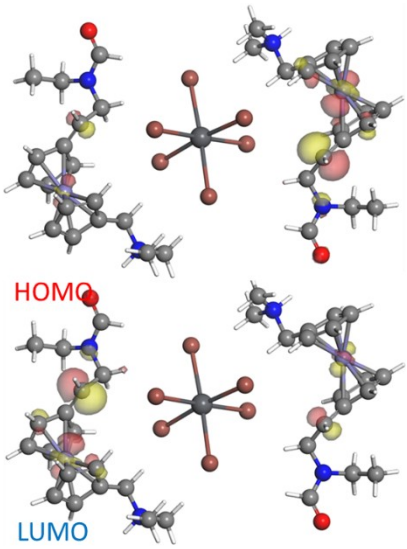

Fig. S9. HOMO and LUMO of $(C_{13}H_{17}FeNH)PbI_3$❿DEF.

Table S1. Crystallographic data for $(C_{13}H_{17}FeNH)PbI_3$ and $(C_{13}H_{17}FeNH)PbI_3$❿DEF.

Empirical formula	$C_{36}H_{58}Fe_2I_6N_4O_2Pb_2$	$C_{13}H_{18}FeI_3NPb$
Formula weight	1866.34	832.02
Temperature/K	296.15	296.16
Crystal system	monoclinic	monoclinic
Space group	$P2_111$	$P112_1$
a/Å	9.7288(14)	9.8348(10)
b/Å	7.9947(11)	8.0487(7)
c/Å	32.946(5)	24.407(2)
α/°	90	90

β/°	89.954(6)	90.033(4)
γ/°	90	90
Volume/Å^3	2562.5(6)	1932.0(3)
Z	2	4
ρ_{calc} g/cm^3	2.419	2.860
μ/mm^{-1}	10.751	14.236
F(000)	1704.0	1480.0
Reflections collected	92763	55997
Independent reflections	11695	6812
R_{int}	0.0300	0.0421
Data/restraints/parameters	11695/1/477	6812/73/346
Goodness-of-fit on F^2	1.183	1.036
Final R indexes [I >=2σ (I)]	R_1 = 0.0154	R_1 = 0.0596
Final R indexes [all data]	R_1 = 0.0169	R_1 = 0.0611

Table S2. Fitting Parameters for TRPL curves of $(C_{13}H_{17}FeNH)PbI_3$ and $(C_{13}H_{17}FeNH)PbI_3$❿DEF.

Perovskites	τ_1 (ns)	A_1	τ_2 (ns)	A_2	τ_{ave} (ns)
$(C_{13}H_{17}FeNH)PbI_3$	0.353	8297.801	0.0131	571.882	0.352
$(C_{13}H_{17}FeNH)PbI_3$❿DEF	0.542	9346.319	0.00141	1029.285	0.541

Table S3. Comparison of various catalysts for photocatalytic oxidation of toluene.

Photocatalyst	Light source	Yield rate ($\mu mol\ g^{-1}\ h^{-1}$)	Selectivity (%)	Ref.
$BiOBr/Bi_2MoO_6$	Blue LED, λ=450 nm	2134.28	87.8	4
Bi_2MoO_6 nanosheets	Xe lamp, λ ≥ 400 nm	778.0	96	5
$Bi_2W_xMo_{1-x}O_6$	Xe lamp, λ ≥ 420 nm	1663	91	6
TiO_2/Bi_2MoO_6	300 W Xe lamp, λ ≥ 400 nm	1036	97	7
(110) Facet-Exposed BiOBr	300 W Xe-lamp	1623	91	8
Bi_2MoO_6-$Bi_2Mo_3O_{12}$	Xe lamp, λ ≥ 400 nm	508	98.5	9
$BiOBr/TiO_2$	Xe lamp, λ ≥ 420 nm	1064	91	10
$Cs_3Bi_2Br_9$	Xe lamp	470	≥88	11
$(C_{13}H_{17}FeNH)PbI_3$	Xe lamp, λ ≥ 420 nm	1600	95.3	This work

References

[1] Guo, K.-K.; Yang, Y.-L.; Dong, S.-M.; Li, F.-Y.; Jiang, X.-Y.; Xu, L. Decomposition-Reassembly Synthesis of a Silverton-Type Polyoxometalate 3D Framework: Semiconducting Properties and Photocatalytic Applications. Inorg. Chem. 2022, 61, 6411-6420.

[2] Dolomanov, O. V.; Bourhis, L. J.; Gildea, R. J.; Howard, J. A. K.; Puschmann, H. OLEX2: a complete structure solution, refinement and analysis program. J. Appl. Crystallogr. 2009, 42, 339-341.

[3] Bourhis, L. J.; Dolomanov, O. V.; Gildea, R. J.; Howard, J. A. K.; Puschmann, H. The anatomy of a comprehensive constrained, restrained refinement program for the modern computing environment-Olex2 dissected. Acta Crystallogr., Sect. A: Found. Adv. 2015, A71, 59-75.

[4] Gu, S.; Li, C.; Lin, X.; Lin, X.; Xiao Y.; Zhao, X.; Nan, J.; Xiao, X. In situ growth of bismuth oxybromide/bismuth molybdate 2D/2D Z-scheme heterojunctions with rich interfacial oxygen vacancies for photocatalytic benzylic C(sp^3)-H bond activation. J. Colloid Interface Sci. 2025, 682, 467-477.

[5] Cai, K.; Lv, S.Y.; Song, L.N.; Chen, L.; He, J.; Chen, P.; Au, C.T.; Yin, S.F. Facile preparation of ultrathin Bi_2MoO_6 nanosheets for photocatalytic oxidation of toluene to benzaldehyde under visible light irradiation, J. Solid State Chem. 2019, 269, 145-150.

[6] Zhang, K.F.; Chen, H. X.; Liu, Y. X.; Deng, J. G.; Jing, L.; Rastegarpanah, A. L.; Pei, W.B.; Han, Z.; Dai, H. X. Two-dimensional $Bi_2W_xMo_{1-x}O_6$ solid solution nanosheets for enhanced photocatalytic toluene oxidation to benzaldehyde, Appl. Catal. B-Environ, 2022, 315, 121545.

[7] Song, L. N.; Ding, F.; Yang, Y. K.; Ding, D.; Chen, L.; Au, C. T.; Yin, S. F.; Synthesis of TiO_2/Bi_2MoO_6 Composite for Partial Oxidation of Aromatic Alkanes under Visible-Light Illumination, ACS Sustain. Chem. Eng. 2018, 6 17044-17050.

[8] Zhou, G. F.; Lei, B.; Dong, F. Lewis Acid Sites in (110) Facet-Exposed BiOBr Promote C-H Activation and Selective Photocatalytic Toluene Oxidation, ACS Catal. 2024, 14, 4791-4798.

[9] Song, L. N.; Chen, L.; He, J.; Chen, P.; Zeng, H. K.; Au, C.T.; Yin, S. F. The first synthesis of Bi self-doped Bi_2MoO_6-$Bi_2Mo_3O_{12}$ composites and their excellent photocatalytic performance for selective oxidation of aromatic alkanes under visible light irradiation, Chem. Commun. 2017, 53, 6480-6483.

[10] Yuan, R. S.; Fan, S. L.; Zhou, H. X.; Ding, Z. X.; Lin, S.; Li, Z. H.; Zhang, Z. Z.; Xu, C.; Wu, L.; Wang, X. X.; Fu, X. Z. Chlorine-Radical-Mediated Photocatalytic Activation of C-H Bonds with Visible Light, Angew. Chem. Int. Edit. 2013, 52, 1035-1039.

[11] Dai, Y.T.; Tüysüz, H. Rapid Acidic Media Growth of $Cs_3Bi_2Br_9$ Halide Perovskite Platelets for Photocatalytic Toluene Oxidation, Sol. Rrl. 2021, 5, 2100265.